J|A|C|S
ARTICLES
Published on Web 07/19/2006

Mössbauer and Computational Study of an N_2-Bridged Diiron Diketiminate Complex: Parallel Alignment of the Iron Spins by Direct Antiferromagnetic Exchange with Activated Dinitrogen

Sebastian A. Stoian,[†] Javier Vela,[‡] Jeremy M. Smith,[‡] Azwana R. Sadique,[‡] Patrick L. Holland,[‡] Eckard Münck,*[,†] and Emile L. Bominaar*[,†]

Contribution from the Department of Chemistry, Carnegie Mellon University, 4400 Fifth Avenue, Pittsburgh, Pennsylvania 15213, and the Department of Chemistry, University of Rochester, Rochester, New York 14627

Received March 24, 2006; E-mail: emunck@cmu.edu; eb7g@andrew.cmu.edu

Abstract: This work reports Mössbauer and DFT studies of the diiron-N_2 complex $L^{Me}FeNNFeL^{Me}$ (L = β-diketiminate), **1a**. Complex **1a**, formally diiron(I), has a system spin $S = 3$ with an isolated $M_S = \pm 3$ quasi-doublet as a ground state; the $M_S = \pm 2$ doublet is >100 cm^{-1} higher in energy. Complex **1a** exhibits at 4.2 K a large, positive magnetic hyperfine field, $B_{int} = +68.1$ T, and an effective g value of 16 ± 2 along the easy magnetization axis of the ground doublet; this value is significantly larger than the spin-only value ($g = 12$). These results have been rationalized by DFT calculations, which show that each Fe site donates significant electron density into the π^* orbitals of dinitrogen, resulting in a configuration best described as two high-spin Fe^{II} ($S_a = S_b = 2$) bridged by triplet N_2^{2-} ($S_c = 1$). In this description the minority spin electron of each iron is accommodated by two nonbonding, closely spaced 3d orbitals, z^2 and yz (z is perpendicular to the diketiminate planes, x is along the Fe···Fe vector). Spin−orbit coupling between these orbital states generates a large unquenched orbital momentum along the iron−iron vector. The $S = 3$ ground state of **1a** results from strong antiferromagnetic direct exchange couplings of the Fe spins ($S_a = S_b = 2$) to the N_2^{2-} spin ($S_c = 1$) and can be formulated as $|((S_a,S_b)S_{ab} = 4, S_c = 1), S = 3\rangle$; $H = J(\mathbf{S}_a + \mathbf{S}_b)\cdot\mathbf{S}_c$ with $J \approx 3500$ cm^{-1}.

1. Introduction

Low-coordinate complexes of the transition metals are a largely uncharted area of coordination chemistry, but more three-coordinate complexes have become available with the use of bulky β-diketiminate ligands (anionic, bidentate ligands that are abbreviated L here).[1] Our collaborative efforts have focused on three-coordinate iron-diketiminate complexes, where the accessibility of variable-temperature, variable-field Mössbauer spectroscopy gives magnetic information that, when combined with density functional theory (DFT), leads to significant insights into electronic structure. Of particular interest to us has been a series of mononuclear complexes (Figure 1) including the iron(II) complexes LFeX (X = Cl, CH_3)[2] and the iron(I) complex LFe(HCCPh).[3] These complexes have electronic ground states that exhibit almost completely unquenched orbital angular momentum in one spatial direction. As a consequence of this unquenching, the ground states (a quasi-doublet for the Fe^{II} complexes and a Kramers doublet for the Fe^{I} compound) display uniaxial magnetic properties with a large g-value and a very large positive magnetic hyperfine field, B_{int}, along the easy axis of magnetization. Moreover, since spin−orbit coupling acts in first-order on the closely spaced orbital pair, the complexes have very large "zero-field splittings", resulting in a ground doublet well separated in energy from the lowest excited magnetic sublevels.[4] In refs 2 and 3 the unusual magnetic

[†] Carnegie Mellon University.
[‡] University of Rochester.

(1) (a) Holland, P. L.; Tolman, W. B. *J. Am. Chem. Soc.* **1999**, *121*, 7270−7271. (b) Randall, D. W.; George, S. D.; Holland, P. L.; Hedman, B.; Hodgson, K. O.; Tolman, W. B.; Solomon, E. I. *J. Am. Chem. Soc.* **2000**, *122*, 11632−11648. (c) Smith, J. M.; Lachicotte, R. J.; Holland, P. L. *Chem. Commun.* **2001**, 1542−1543. (d) Holland, P. L.; Cundari, T. R.; Perez, L. L.; Eckert, N. A.; Lachicotte, R. J. *J. Am. Chem. Soc.* **2002**, *124*, 14416−14424. (e) Spencer, D. J. E.; Reynolds, A. M.; Holland, P. L.; Jazdzewski, B. A.; Duboc-Toia, C.; Le Pape, L.; Yokota, S.; Tachi, Y.; Itoh, S.; Tolman, W. B. *Inorg. Chem.* **2002**, *41*, 6307−6321. (f) Eckert, N. A.; Bones, E. M.; Lachicotte, R. J.; Holland, P. L. *Inorg. Chem.* **2003**, *42*, 1720−1725. (g) Puiu, S. C.; Warren, T. H. *Organometallics* **2003**, *22*, 3974−3976. (h) Chai, J.; Zhu, H.; Fan, H.; Roesky, H. W.; Magull, J. *Organometallics* **2004**, *23*, 1177−1179. (i) Eckert, N. A.; Smith, J. M.; Lachicotte, R. J.; Holland, P. L. *Inorg. Chem.* **2004**, *43*, 3306−3321. (j) Vela, J.; Stoian, S.; Flaschenriem, C. J.; Münck, E.; Holland, P. L. *J. Am. Chem. Soc.* **2004**, *126*, 4522−4523. (k) Chai, J.; Zhu, H.; Roesky, H. W.; He, C.; Schmidt, H.-G.; Noltemeyer, M. *Organometallics* **2004**, *23*, 3284−3289. (l) Vela, J.; Vaddadi, S.; Cundari, T. R.; Smith, J. M.; Gregory, E. A.; Lachicotte, R. J.; Flaschenriem, C. J.; Holland, P. L. *Organometallics* **2004**, *23*, 5226−5239. (m) Dai, X.; Warren, T. H. *J. Am. Chem. Soc.* **2004**, *126*, 10085−10094. (n) Kogut, E.; Zeller, A.; Warren, T. H.; Strassner, T. *J. Am. Chem. Soc.* **2004**, *126*, 11984−11994. (o) Chai, J.; Zhu, H.; Stueckl, A. C.; Roesky, H. W.; Magull, J.; Bencini, A.; Caneschi, A.; Gatteschi, D. *J. Am. Chem. Soc.* **2005**, *127*, 9201−9206. (p) Eckert, N. A.; Stoian, S.; Smith, J. M.; Bominaar, E. L.; Münck, E.; Holland, P. L. *J. Am. Chem. Soc.* **2005**, *127*, 9344−9345. (q) Kogut, E.; Wiencko, H. L.; Zhang, L.; Cordeau, D. E.; Warren, T. H. *J. Am. Chem. Soc.* **2005**, *127*, 11248−11249. (r) Eckert, N. A.; Dinescu, A.; Cundari, T. R.; Holland, P. L. *Inorg. Chem.* **2005**, *44*, 7702−7704.
(2) Andres, H.; Bominaar, E. L.; Smith, J. M.; Eckert, N. A.; Holland, P. L.; Münck, E. *J. Am. Chem. Soc.* **2002**, *124*, 3012−3025.

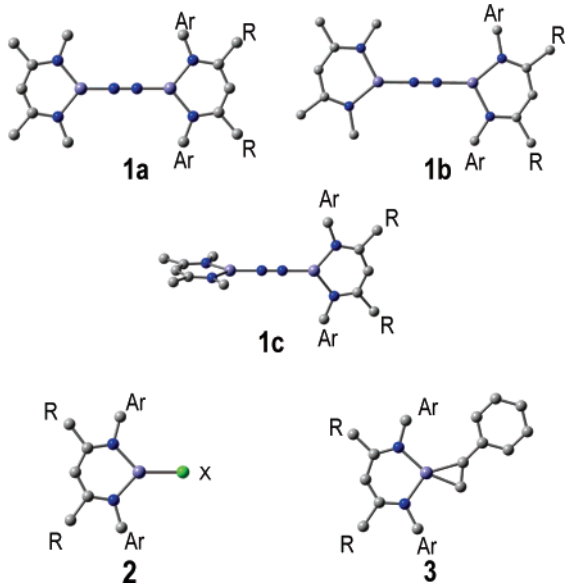

Figure 1. Schematic representation of the X-ray structures of: **1a**, idealized D_{2h} LFeNNFeL, R = Me; **1b**, idealized C_{2h} LFeNNFeL, R = Me; **1c**, idealized D_{2d} LFeNNFeL, R = ^{t}Bu; **2**, LFe^{II}X where X = Cl, Me, and R = ^{i}Pr; **3**, LFe^I(HCCPh) where R = ^{t}Bu and Ar = (2,6-di-^{i}Pr)Ph. Note that in **1b** the diketiminates are rotated by ca. 22° relative to the Fe−N−N−Fe axis.

properties were attributed to a quasi-degenerate, nonbonding $\{z^2,yz\}$ pair that accommodates a total of three electrons.

In ref 3, the reason for the strikingly similar magnetic properties of the analogous iron(I) and iron(II) complexes was elucidated by DFT studies. In short, the *xy* orbital is high in energy (singly occupied) in iron(II) complexes and low in energy (doubly occupied) in the iron(I) complex, leaving the occupation of the quasi-degenerate $\{z^2,yz\}$ pair the same in both complexes. The precipitous drop in energy of the *xy* orbital in the iron(I) complex arises from strong back-bonding into an unoccupied π^* orbital of the acetylene ligand. These calculations also showed that the easy axis of magnetization, labeled *x*, is in the Fe−diketiminate plane and directed toward the nondiketiminate ligand, roughly along the bisector of the N−Fe−N angle (*z* is perpendicular to the diketiminate plane).

Building from our understanding of these mononuclear complexes, we now address diiron complex **1a** in which N_2 bridges two formally iron(I) ions in an LFeNNFeL core. For this compound, crystallographic and spectroscopic evidence indicates that the N_2 ligand is somewhat reduced: the N−N bond length is increased relative to N_2 (1.186 Å vs 1.098 Å) and the N−N stretching frequency is decreased (1810 cm^{-1} vs 2331 cm^{-1}).[5−7] Three crystalline forms of LFeNNFeL are available. Using β-diketiminate ligands with R = CH_3 (Figure 1, **1a** and **1b**) we have obtained two polymorphs of L^{Me}FeNNFeL^{Me}; in both forms the two iron−diketiminate planes are coplanar,[7] in contrast to the nearly perpendicular planes observed for L^{tBu}FeNNFeL^{tBu} (R = ^{t}Bu, **1c**).[5] In the present paper we will focus mainly on the highly symmetric structure L^{Me}FeNNFeL^{Me} (**1a**) which has idealized D_{2h} symmetry (real C_{2h}). Structure **1a** may be distorted, apparently by crystal packing forces,[7] to yield planar **1b** in which the bisector of diketiminate ligands is shifted by 20−25° off the Fe−N−N−Fe axis; the Mössbauer spectrum of Figure 2A was obtained from a single crystal of **1b**.

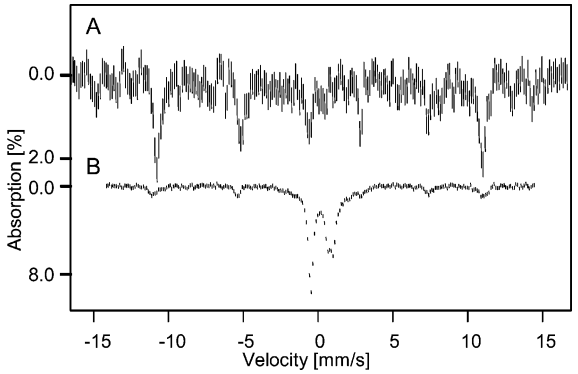

Figure 2. (A) Mössbauer spectrum for a single crystal of **1b** recorded at 4.2 K in a 0.05 T applied field; the crystal contained ^{57}Fe in natural abundance (2.2%). (B) Mössbauer spectrum for a polycrystalline powder of **1a**, an earlier sample, recorded at 4.2 K, 0.05 T.

1a−**c** are formally diiron(I) complexes, and thus they are non-Kramers systems with integer or zero electronic spin. For reasons well understood,[8] low-temperature Mössbauer spectra of non-Kramers systems, recorded in the absence of an applied magnetic field, generally lack magnetic features. Thus, we were surprised to observe that the spectra of **1a**−**c**, and **2** each exhibited paramagnetic hyperfine structure in zero-applied field, in the solid as well as in frozen solution. Two additional observations were particularly puzzling, namely (1) the Mössbauer spectral features indicated the presence of orbital degeneracies similar to those reported for LFe^I(HCCPh),[3] and LFe^{II}−X,[2] and (2) the spectra of **1** revealed parallel alignment of the spins of the two iron sites. Observation (2) suggested ferromagnetic coupling. However, inspections of exchange pathways in **1a**−**c** indicate that antiferromagnetic coupling between the two iron sites should be dominant.

In this paper we present detailed Mössbauer studies of complex **1a** and demonstrate with the aid of DFT calculations that the observed orbital degeneracies, again, involve the $\{z^2,yz\}$ pair. The DFT calculations reveal substantial unpaired spin density on the dinitrogen moiety as a result of back-donation into empty π^* orbitals of the dinitrogen. We will show that the parallel alignment of the iron spins is not due to ferromagnetic interactions between the iron sites but results from direct, antiferromagnetic exchange between each iron and the bridging dinitrogen dianion. Our theoretical analysis suggests that **1a** is perhaps best described as a diiron(II) complex ($S_a = S_b = 2$) bridged by an $S_c = 1$ dinitrogen dianion.

(3) Stoian, S. A.; Yu, Y.; Smith, J. M.; Holland, P. L.; Bominaar, E. L.; Münck, E. *Inorg. Chem.* **2005**, *44*, 4915−4922.
(4) For the LFe^{II}CH$_3$ complex the quasi-degenerate ground doublet has $S = 2$ and $M_S = \pm 2$; the next spin sublevels are at energies larger than 150 cm^{-1}. For the high-spin LFe^I(HCCPh), **3**, complex the $S = {}^3/_2$, $M_S = \pm {}^3/_2$ Kramer's doublet is lowest in energy and the energy gap between the two lowest doublets (the "zero-field splitting" of the $S = {}^3/_2$ multiplet) is approximately 170 cm^{-1}).
(5) Smith, J. M.; Lachicotte, R. J.; Pittard, K. A.; Cundari, T. R.; Lukat-Rodgers, G.; Rodgers, K. R.; Holland, P. L. *J. Am. Chem. Soc.* **2001**, *123*, 9222−9223.
(6) Holland, P. L. *Can. J. Chem.* **2005**, *83*, 296−301.
(7) Smith, J. M.; Sadique, A. R.; Cundari, T. R.; Rodgers, K. R.; Lukat-Rodgers, G.; Lachicotte, R. J.; Flaschenriem, C. J.; Vela, J.; Holland, P. L. *J. Am. Chem. Soc.* **2006**, *128*, 756−769.
(8) (a) Münck, E. *Methods Enzymol.* **1978**, *54*, 346−379. (b) Münck E., *Physical Methods in Inorganic and Bioinorganic Chemistry*; University Science Books: Sausolito, CA, 2000; Chapter 6, pp 287−319. (c) Münck E., In *The Porphyrins*; D. Dolphin, Ed.; Academic Press: New York, 1979; Vol. IV, Chapter 8.

2. Materials and Methods

Compounds **1a** and **1b** were synthesized according to literature methods[5,7] and were suspended in Nujol or Krytox oils in the Mössbauer cells. Because these compounds are *highly* air- and moisture sensitive, they were shipped, stored, and analyzed in specially designed Delrin cells with tight-fitting caps (shrink fits), which were kept at 77 K during transport from Rochester to Pittsburgh inside capped test tubes.

As described in ref 7, there are two crystal modifications of L^{Me}-$FeNNFeL^{Me}$. Crystals grown from pentane solution at low temperature contained pentane solvate and had a highly symmetrical D_{2h} core, while a very large crystal grown from pentane solution at room-temperature had a crystal structure in which the diketiminate ligands remain in the same plane, but are twisted as shown in Figure 1 (**1b**). The crystal structure determination[7] and Mössbauer measurements of **1b** used chips of the same crystal; the one used for Mössbauer studies was cut to a size of approximately 4 mm × 4 mm × 2 mm to fit in the cell. Mössbauer spectra were recorded on two spectrometers, using Janis Research Super-Varitemp dewars that allowed studies in applied magnetic fields up to 8.0 T in the temperature range from 1.5 to 200 K. Mössbauer spectral simulations were performed using the WMOSS software package (WEB Research, Edina, MN). The relaxation analysis was performed using stochastic line-shape theory as implemented by Schulz and co-workers.[9] Isomer shifts are quoted relative to Fe metal at 298 K.

The DFT calculations and geometry optimizations were performed with Gaussian '03, using the functional B3LYP, basis set 6-311G, and default setting for the convergence criteria. Estimates for 3d excitation energies were obtained from time-dependent (TD) DFT calculations. Details of the calculations are presented in the Supporting Information.

3. Results

3.1. Preliminary Remarks. The 4.2 K Mössbauer spectrum of a polycrystalline sample of **1a** (Figure 2B), recorded in a parallel applied field of 50 mT, exhibits at least two subspectra: a magnetic component (a six-line spectrum extending over a velocity range of 22 mm/s) and one, or perhaps two, quadrupole doublets. The six-line spectrum is observed even in the absence of an applied magnetic field. This property is a typical attribute of systems with half-integral electronic spin; yet none of the samples exhibited an EPR signal. Since **1a** has an even number of electrons, we initially suspected that the central quadrupole doublet(s) in Figure 2B was the signature of **1a**. Samples of **1a** were, for reasons not yet fully understood, quite unstable, and some samples did not last longer than a few weeks under storage at 77 K. Interestingly, it always was the paramagnetic component that decayed, accompanied by increased intensity of the central quadrupole doublet(s), and thus we suspected that it was the magnetic component that represented **1a**. To further support our suspicion that this component indeed represents the diiron(I) complex, we studied a single crystal of **1b**. Its Mössbauer spectrum, shown in Figure 2A, exhibits only the six-line magnetic feature, showing that the six-line pattern represents complex **1**. (A chip of the ca. 4 × 4 × 2 mm^3 single crystal was studied by crystallography; in this experiment we discovered that $L^{Me}FeNNFeL^{Me}$ can crystallize, under suitable conditions, in form **1b**, see Materials and Methods section.) The sample of **1a** studied in the following section is a polycrystalline sample from a batch different from that of Figure 2A; it had the highest fraction of iron in the magnetic component (77%), and its Mössbauer spectra were recorded immediately upon arrival of the sample in Pittsburgh.

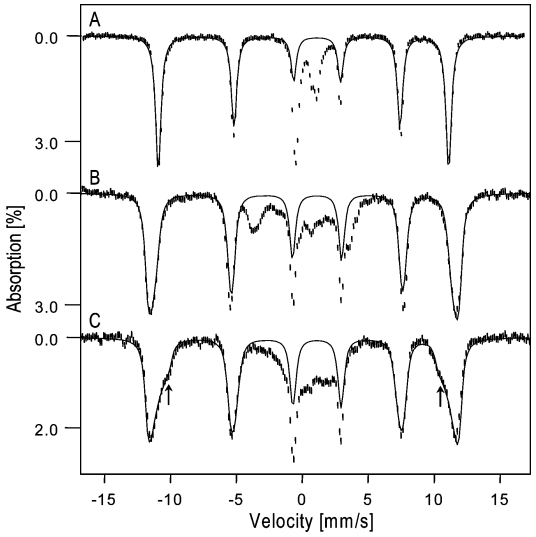

Figure 3. Mössbauer spectra of a sample from ground crystals for **1a**. (A) 4.2 K, 0.05 T; (B) 4.2 K, 6.0 T; (C) 40 K, 6.0 T. The parameters used for the fits (solid lines) are: $\Delta E_Q = +1.41$ mm/s, $\delta = 0.62$ mm/s, $\eta = -0.54$, 0.5 mm/s full width at half-maximum, $A_x/g_n\beta_n = +68.1$ T, $A_y = A_z = 0$, $g_x = 16.0$ and $g_y = g_z = 0$.

To gain insight into the electronic structure of **1a**, we have first studied a mononuclear Fe(I) diketiminate complex, LFe-phenylacetylene, **3**, with Mössbauer and EPR spectroscopy as well as by DFT calculations.[3] The ground state of **3** is a Kramers doublet with effective *g*-values $g_x = 8.9$ and g_z, $g_y < 0.3$. This doublet produces a Mössbauer spectrum characterized by a very large and *positive* internal magnetic field at the iron nucleus, $B_{int} = +68.8$ T. Analysis of Mössbauer relaxation spectra has shown that the ground doublet is separated from the first excited state, a member of the same spin manifold to which the ground doublet belongs, by as much as 110−180 cm^{-1}. These properties have been attributed to an orbital degeneracy, which allows spin−orbit coupling to generate orbital angular momentum in one spatial direction. The ground doublet of **3** was identified as the state $|S = {}^3/_2, M_S = \pm {}^3/_2\rangle$ (In refs 2 and 3 the spin was quantized along *x*, with *z* perpendicular to the diketiminate plane; we will adopt the same convention here.). Assuming degeneracy between z^2 and *yz*, the expectation values of the *x*-component of orbital angular momentum, $\langle L_x \rangle$, in the $M_S = \pm {}^3/_2$ doublet is $\pm\sqrt{3}$, yielding $g_x = 2(3 + \sqrt{3}) = 9.5$ and $B_{L,x} \approx +100$ T for the $M_S = -{}^3/_2$ level, where $B_{L,x}$ is the orbital contribution[10] to the internal field at the Fe nucleus, B_{int} (the negative Fermi contact contribution reduces B_{int} to about +70 T).

3.2. Mössbauer Studies of $L^{Me}FeNNFeL^{Me}$, 1a. Figure 3A shows a 4.2 K spectrum of polycrystalline **1a** recorded in a parallel field of 50 mT. The splitting of the six-line pattern corresponds to a magnetic hyperfine field of $B_{int} = +68.1(3)$ T, among the largest observed for any Fe complex.[2,3,11,12] The

(9) Schulz, C. E.; Nyman, P.; Debrunner, P. G. *J. Chem. Phys.* **1987**, *87*, 5077−5091.

(10) Abragam, A.; Bleaney, B. *Electron Paramagnetic Resonance of Transition Ions*; Clarendon Press: Oxford, 1970; Chapter 17.

(11) Reiff, W. M.; LaPointe, A. M.; Witten, E. H. *J. Am. Chem. Soc.* **2004**, *126*, 10206−10207.

(12) Reiff, W. M.; Frommen, C. M.; Yee, G. T.; Sellers, S. P. *Inorg. Chem.* **2000**, *39*, 2076−2079.

(magnetically split) spectra for the two sites of **1a** are indistinguishable, in accord with the X-ray structure which indicates an idealized D_{2h} symmetry. Since **1a** has integer electronic spin and exhibits a six-line pattern in zero field (see Figure S5), the electronic ground state must be a (quasi-degenerate) non-Kramers doublet (the splitting Δ between the two levels of the doublet is less than 0.001 cm^{-1}, see Discussion). We will describe the magnetic properties of this doublet with a fictitious spin $S = {}^1/_2$, using for the simulation of the Mössbauer spectra the Hamiltonian,

$$\mathscr{H} = \beta \mathbf{S}\cdot\mathbf{g}\cdot\mathbf{B} + \mathbf{S}\cdot\mathbf{A}\cdot\mathbf{I} - g_n\beta_n\mathbf{B}\cdot\mathbf{I} + \mathscr{H}_Q \qquad (1)$$

where $\mathscr{H}_Q$ describes the quadrupole interactions of the nuclear excited state, **g** describes the Zeeman splitting of the electronic ground doublet, and the **A**-tensor accounts for the magnetic hyperfine splitting; since the two iron sites are identical (by crystallographic and Mössbauer evidence), it suffices to calculate one spectrum. The intensities of the absorption lines of the 50 mT spectra of **1a** do not depend on the direction (parallel vs perpendicular to the γ-beam) of the applied field B, showing that **g** in eq 1 is extremely anisotropic.[8a] From the shape of the absorption lines we can conclude, aided by spectral simulations based on eq 1, that g_x is at least 20 times larger than g_z and g_y.[13] For larger values of g_z and g_y, B_{int} ($= -\langle \boldsymbol{S}\rangle\cdot\mathbf{A}/g_n\beta_n$) would diverge from the x-direction for molecular orientations for which the applied field is close to the molecular yz plane, causing a tailing of the absorption lines toward smaller velocities. For the spectral simulations we have adopted $g_y = g_z = 0$.

Figure 3B shows a 4.2 K spectrum of **1a** recorded in a field of 6.0 T applied parallel to the γ beam. The magnetic splitting has increased relative to that of the 50 mT spectrum of Figure 3A, showing that B_{int} is positive, i.e., parallel to the applied field for essentially all molecular orientations. It is noteworthy that B_{int} of complex **1a** is identical to that of mononuclear complex **3** suggesting that **1a** is a system, perhaps coupled in an unusual way, whose mononuclear components have electronic ground states with the same $z^2 - yz$ degeneracy as those of **3**.

The spin-up and spin-down states of the ground doublet of **1a** are associated with internal magnetic fields of equal magnitude but opposite sign. Thus, for $B = 6.0$ T the effective field at the nucleus for the spin-down level will increase by 6.0 T (for molecular orientations for which B is along the molecular x axis) and decrease by 6.0 T for the spin-up state. For slow spin relaxation we should observe two Mössbauer spectra with intensities governed by the Boltzmann factor, which is determined by the Zeeman splitting of the doublet. The relative intensities of the two spectral components have been used to obtain an estimate for g_x. Figure 3C shows a 6.0 T spectrum of **1a** recorded at 40 K. Population of the spin-up state is apparent by the shoulders (arrows) that are lacking in the 4.2 K spectrum of Figure 3B. From a fit to the spectrum of Figure 3C we estimate $g_x = 16 \pm 2$. Significantly the Zeeman splitting of **1a** is twice as large as that of **3**, suggesting that the ground doublet of **1a** comprises the product of the $M_S = \pm{}^3/_2$ states of mononuclear **3** and thus appears to belong to an $S = 3$, $M_S = \pm 3$ manifold. Finally, it should be noted that the observation of spin-up and spin-down states rules out the possibility that the magnetic features observed in the 4.2 K zero-field spectra of **1a** are the result of long-range magnetic order as would occur, for instance in a bulk ferromagnet.

The D_{2h} symmetry of **1a** requires that one of the principal axes of the electric field gradient (EFG) tensor is parallel to B_{int}. The spectrum of Figure 3A shows that the component of the EFG along B_{int} is negative, $eQV_{xx}/2 = -1.00$ mm/s. At 170 K where the spin fluctuation rate approaches the fast relaxation limit (see below) we obtained the value $\Delta E_Q = 1.41$ mm/s for the quadrupole splitting of **1a**. We have no evidence that ΔE_Q is temperature dependent (this is supported by the analysis given in section 4.4.2), and therefore, using the 170 K value, we obtain for the asymmetry parameter of the EFG the value $\eta \approx 0.48$. Thus, the largest component of the EFG, $eQV_{zz}/2 = +1.35$ mm/s, is perpendicular to B_{int}; $\Delta E_Q = (eQV_{zz}/2)(1+\eta^2/3)^{1/2}$. Finally, the isomer shift of **1a**, the centroid of the Mössbauer spectrum, is $\delta = 0.62$ mm/s at 4.2 K, relative to Fe metal at 298 K. (Since the magnetic hyperfine field is uniaxial along x, the EFG tensor can be rotated freely around x without effecting the Mössbauer spectrum. We have placed z along the largest component of the EFG; this agrees with the DFT calculations of Table 2.)

Approximately 77% of the absorption in Figure 3A belongs to complex **1a**. The remainder is associated with two quadrupole doublets with $\Delta E_Q = 1.5$ mm/s, $\delta = 0.34$ mm/s (16%) and $\Delta E_Q = 1.12$ mm/s, $\delta = 0.13$ mm/s (7%), both representing decay products. It can be seen that five lines of **1a** have no overlap with the features of the contaminants. Since knowledge of five lines of the six-line spectrum completely determines position and intensity of the sixth line, we can subtract the spectrum **1a** using its simulation to prepare a spectral representation of the contaminants. We have no evidence that the quadrupole splittings of the contaminants are temperature dependent, and therefore we have subtracted the spectrum thus prepared from all 50 mT spectra shown below in Figure 4, applying minor corrections for second-order Doppler shifts. We do not know the nature of the contaminants, but the data of Figure 3 show that they are integer spin paramagnets.

As the temperature is raised above 4.2 K, the 50 mT Mössbauer spectra of **1a** pass through two different regimes of electronic relaxation. At 170 K the electronic spin approaches the fast fluctuation limit, and the Mössbauer spectrum consists of a quadrupole doublet with $\Delta E_Q = 1.41(1)$ mm/s and $\delta = 0.58(1)$ mm/s. As shown in Figure 4 the magnetic splitting of **1a** declines by ca. 1% between 4.2 and 55 K. Such behavior (commonly) is characteristic of a system for which the electronic spin makes rapid transitions between one member of the ground state and some excited state(s). For instance, if the ground doublet of **1a** would be the $M_S = \pm 3$ doublet of an isolated $S = 3$ multiplet, the observed temperature dependence of B_{int} would involve fast relaxation in the ladders $M_S = -3 \leftrightarrow -2 \leftrightarrow -1$ etc. and $M_S = +3 \leftrightarrow +2 \leftrightarrow +1$ etc. (We have analyzed in some detail a similar situation for an $Fe^{II}Fe^{III}$ dimer.[14]) We do not yet have sufficient information (but see section 4.4.2) about the excited states of **1a** to analyze the temperature dependence

(13) We will use a coordinate system for which the xy plane coincides with the diketiminate planes of **1a**, with x along Fe−N−N−Fe. We will show below that the easy magnetic axis of the ground doublet of **1a** is along x. For this reason we quantize the fictitious spin along x, i.e., $S_x|+{}^1/_2\rangle = +{}^1/_2|+{}^1/_2\rangle$. This nomenclature conforms to that of refs 2 and 3.

(14) Stubna, A.; Jo, D.-H.; Costas, M.; Brenessel, W. W.; Andres, H.; Bominaar, E. L.; Münck, E.; Que, L., Jr. *Inorg. Chem.* **2004**, *43*, 3067−3079.

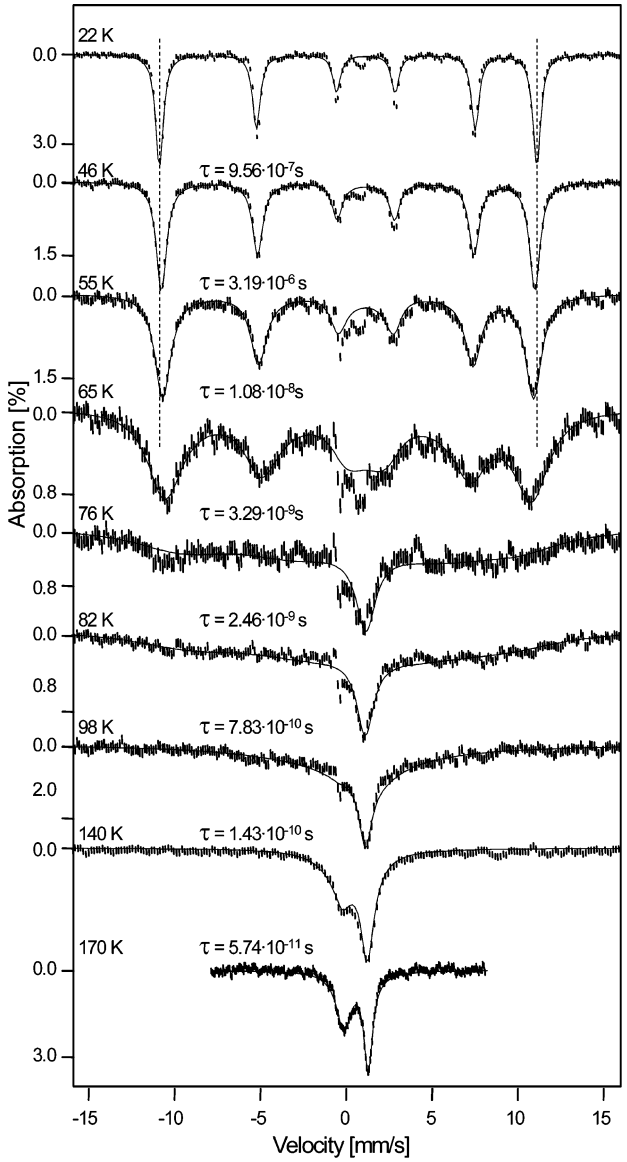

Figure 4. Variable-temperature Mössbauer spectra of **1a** recorded in parallel field of 0.05 T. $1/\tau$ is the stochastic flip rate of the electronic spin. The two vertical dotted lines illustrate the decrease of B_{int} with the temperature. The simulations were performed using $\Delta E_Q = 1.41$ mm/s, $\eta = 0.48$, $A_y = A_z = 0$, A_x variable, and $g_x = 16$, $g_y = g_z = 0$.

of B_{int}; for completeness, we quote the temperature dependence of this quantity: 4.2 K, 68.1(2) T; 22 K, 68.1(2) T; 34 K, 67.8-(2) T; 46 K, 67.4(3), 55 K, 67.0(3) T.

Above 55 K the Mössbauer spectra of **1a** broaden considerably and the spectral features are typical of a system passing from slow ($\tau > 10^{-6}$ s) to fast ($\tau < 10^{-10}$ s) paramagnetic relaxation, involving effective spin flips, with rate $1/\tau$, between the spin-up and spin-down members of the ground doublet. Wickmann[15] has described a model, developed from the theory of chemical exchange in NMR spectroscopy, that describes the fluctuation of B_{int} by a single relaxation parameter, τ. We have employed this model, using a program described by Schulz et al.[9] to fit the spectra of Figure 4. The values of τ used for generating the theoretical curves are listed in the Figure 4. The spectra obtained at 4.2 and 22 K have identical line width; at this temperatures the width of the absorption lines (~0.5 mm/s full width at half-maximum) is dominated heterogeneous broadening caused by a distribution of B_{int} and not by (homogeneous) broadening due to relaxation.

If the ground-state complex **1a** would be an isolated $S = 3$ spin multiplet describable by a quadratic spin Hamiltonian DS_x^2, the temperature dependence of the Mössbauer spectra could be understood as follows:[16] At temperatures below ~55 K the electronic spin undergoes rapid ($\Delta M_S = \pm 1$) transitions involving the $M_S = -3 \leftrightarrow -2 \leftrightarrow -1$ etc. and $M_S = +3 \leftrightarrow +2 \leftrightarrow +1$ ladders. The number of transitions between two levels is proportional to the (temperature-dependent) transition rate and the population of the levels involved; the latter is given by the Boltzmann factor. For $kT < |D|$ transitions involve essentially the two lowest states in each ladder, and the system rarely crosses over to levels with M_S values of opposite sign. It is important to recall that in such a system the B_{int} associated with each electronic level is proportional to $\langle S_x \rangle$. In ref 14 we used this model to determine the zero-field splitting parameter D of the $S = {}^9/_2$ ground multiplet of a ferromagnetically coupled Fe^{II}-Fe^{III} dimer. If we adopt (unjustified as we shall see in section 4.4) the same procedure for a presumed $S = 3$ ground multiplet, we find that the $M_S = \pm 2$ levels are at 110 cm^{-1}, implying a very large zero-field splitting for **1a**. In the relaxation process commencing above 55 K, involving an effective flip rate $1/\tau$ between the members of the ground doublet, the system might climb up one branch of the spin ladder, cross over at $M_S = 0$, and run down the other branch. Since the population of the higher-energy levels is exceedingly small below 60 K, the time τ required for the $M_S = \pm 3 \leftrightarrow M_S = \mp 3$ flips is expected to be long.

There are two problems with the above picture as applied to **1a**. The analysis presented in the Discussion section show that the energy levels of the $S = 3$ multiplet do not have the spacings predicted by the commonly used zero-field splitting term but follow a quasi-linear pattern (see Figure 8A below). Moreover, in systems with isolated ground multiplets described by DS_z^2, B_{int} of each level of the ground spin multiplet is proportional to the expectation value of the spin, because in systems with essentially quenched orbital angular momentum the orbital contribution to the **A**-tensor enters in second-order perturbation by a cross-term involving spin−orbit coupling and the orbital part of the magnetic hyperfine operator (see eqs 19.9 and 19.32 of Abragam and Bleaney[10]). For systems with unquenched orbital angular momentum, in contrast, the (large) orbital part of the magnetic hyperfine field, $\mathbf{B}_L$, is proportional to $\langle \mathbf{L} \rangle$, not to $\langle \mathbf{S} \rangle$. In that case, B_{int} contains a contribution proportional to $\langle \mathbf{S} \rangle$ (spin-dipolar and Fermi contact) and a term proportional to $\langle \mathbf{L} \rangle$, and thus these considerations show that understanding of the temperature dependence of B_{int} requires knowledge of $\mathbf{B}_L$ not only for the ground state but also for excited states with different orbital angular momentum. We will comment on this point in section 4.4.2.

Figure 5 shows a plot of $\log(1/\tau)$ versus $1/T$. We have analyzed the spin-flip rate $1/\tau$ using eq 2 (eq 1.139 of ref 10)

(15) (a) Wickman, H. H.; Wertheim, G. K. In *Chemical Applications of Mössbauer Spectroscopy*; Goldanskii V. I., Herber, R. H., Eds.; Academic Press: New York, 1968. (b) Wickman, H. H.; Klein, M. P.; Shirley, D. A. *Phys. Rev.* **1966**, *152*, 345−357.

(16) The reader may forgive us for presenting, twice, the wrong model. However, these models were the most obvious, and their flaws needed to be revealed before developing the correct model, we hope, for this unusual compound.

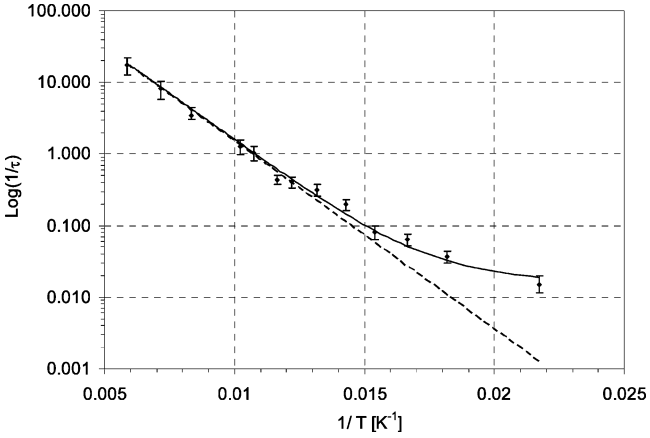

Figure 5. Relaxation rate plotted as a function of temperature. The solid line is a fit to eq 2 for $a = 1.2 \times 10^{-5}$ GHz, $b = 6.6 \times 10^{2}$ GHz and $\Delta = 420$ cm^{-1}. The dashed line corresponds to an Orbach process with $\Delta = 420$ cm^{-1}.

where the first and second term describe the direct and Orbach process, respectively.

$$\frac{1}{\tau} = a \coth\left(\frac{h\nu}{2kT}\right) + \frac{b}{\exp\left(\frac{\Delta}{kT}\right) - 1} \qquad (2)$$

In eq 2, a and b are adjustable constants, $h\nu$ is the Zeeman splitting of the ground state, and Δ is the energy of an excited state that can transiently be populated by phonon absorption from one member of the ground doublet, followed by phonon emission to the other member of the ground doublet. The plot in Figure 5 seems to suggest $\Delta \approx 420$ cm^{-1}. For complex **3** the Orbach process identified involved transitions from the $M_S = \pm 3/2$ ground doublet to the $M_S = \pm 1/2$ levels.[3] For complex **1a** we cannot as yet identify an excited state at energy $\Delta = 420$ cm^{-1}. The relaxation pathway for **1a** may involve various sequential processes involving phonon energies of the order 200 cm^{-1} (see energy spacings in Figure 8 below), and the quantity Δ of Figure 5 may reflect an average of these processes. We do not yet have sufficient information about **1a** to interpret the results of Figure 5 with confidence, and we defer further discussion to future work.

4. Theoretical Analysis and Discussion

4.1. Preliminary Considerations. In this section we explore the interpretation of the Mössbauer results obtained for complex **1a**. First, we consider our results from a phenomenological perspective. This approach suggests parallel coupling of the spins of two Fe^{I} sites and would imply that we are dealing with an uncommon phenomenon, namely that of ferromagnetic exchange in a linear bridge. This enigma is resolved in the next section using the results obtained from an extensive DFT study which shows that substantial spin-down density is transferred from the iron to the bridging nitrogen through back-bonding into empty π^* orbitals, suggesting that the system might better be described as a diferrous complex bridged by a spin-triplet N_2^{2-} moiety. In the ensuing 3-spin model parallel coupling of the iron spins results from strong antiferromagnetic direct exchange between the Fe^{II} sites ($S_a = S_b = 2$) and N_2^{2-} ($S_c = 1$). While DFT provides substantial insight into the electronic structure of **1a**, it is not suitable to explain the uniaxial magnetic properties of the ground doublet. To properly describe the unquenching of the orbital momentum by spin−orbit coupling, one would need a quantum chemical approach that yields state energies with accuracy on the order of 100 cm^{-1} which is beyond the present accuracy of DFT (ca. 1500 cm^{-1}). Instead, using the DFT results as a guide, we have used a crystal-field approach, eq 4 below, that takes into account the crystal field, spin−orbit coupling and direct exchange between the iron sites and N_2^{2-}. This approach enables us to explore the conditions that give rise to the observed magnetic properties.

4.2. Assessment of Spin Coupling. The high-spin LFe^{I}-phenylacetylene complex, **3**, is a suitable mononuclear model that provides crucial insight into the electronic structure of the metal sites in **1a**. Thus, the iron sites of both **1a** and **3** have one non-diketiminate ligand with low-lying empty π^* orbitals, and for both complexes the z^2 and yz orbitals are essentially nonbonding (as they are in the Fe^{II} complex **2**), preserving the orbital degeneracy that has a strong imprint on the spectroscopic properties of the systems. Back-bonding into π^* removes substantial electron density from the iron, leading to an electronic configuration in which one β spin is allocated to the z^2/yz orbitals. The degeneracy of z^2 and yz in the Fe^{I} complex **3** yielded the expectation value $\langle L_x \rangle = +\sqrt{3}$ for the "spin down" level of the ground doublet[3] and thus a very large positive contribution to the internal magnetic field sensed by Mössbauer spectroscopy, $B_{L,x} = \sqrt{3}$ P, with $P = 2\beta\langle r^{-3}\rangle$.[10] Moreover, the orbital degeneracy in **3** creates an anisotropic ground Kramers doublet with maximum $g_x = 2(3 + \sqrt{3}) = 9.4$ (experimental: $g_x = 8.9$). Analysis of the Mössbauer spectra of Figure 2 yielded $g_x = 16 \pm 2$ which, within the uncertainties, is about twice the $g_x = 8.9$ observed for the mononuclear **3**.

Although **1a** has integer electronic spin, the Mössbauer spectra exhibit paramagnetic hyperfine structure in zero field (Figure S5), implying that the electronic ground state must be a (quasi) doublet with a splitting, Δ, smaller than the magnetic hyperfine interactions; roughly $\Delta < 0.001$ cm^{-1} (see below). For the remainder of this paragraph we will assume, as seems to be the case, that the ground Kramers doublets of the local sites of **1a** are similar to that observed[3] for monomer **3**. It will be instructive, although not quite correct as we shall see, to describe the magnetic properties of the quasi-doublet of **1a** with an Ising-type Hamiltonian, eq 3, that couples the ground Kramers doublets (effective spins $S'_{a,x} = S'_{b,x} = 1/2$) of the local sites a and b.

$$\mathscr{H} = J_x S_{a,x} S_{b,x} + g_{a,x}\beta B_x S_{a,x} + g_{b,x}\beta B_x S_{b,x} \qquad (3)$$

J_x is a constant describing the exchange coupling; $J_y = J_z = 0$ and $g_{a,y} = g_{a,z} = 0$ (the symmetry of **1a** implies $g_a = g_b$).[17] For ferromagnetic coupling, $J_x < 0$, eq 3 yields for the coupled

(17) In the case that the metal sites have negative, axial zero-field splittings, $D_{a,x} = D_{b,x} < 0$, the ground manifold of the dimer is given by the quartet $|\pm 3/2\rangle_a|\pm 3/2\rangle_b$. Since the last two terms of the Heisenberg−Dirac−van Vleck operator, $J\boldsymbol{S}_a\cdot\boldsymbol{S}_b = J(S_{a,x}S_{b,x} + S_{a,y}S_{b,y} + S_{a,z}S_{b,z})$, have vanishing matrix elements in the quartet space, the HDvV operator reduces to the Ising Hamiltonian $JS_{a,x}S_{b,x}$ in this space; recall that we have quantized the spin along x. The Ising Hamiltonian is only meaningful when the off-diagonal interactions of the HDvV operator between the ground quartet and the excited zero-field levels, $|M_S| < 3/2$, are small compared to the energies separating these levels. This condition is fulfilled when $|D| \gg |J|$. We refer to papers by Mironov and co-workers for an in-depth discussion of the Ising Hamiltonian. (a) Mironov, V. S.; Chibotaru, L. F.; Ceulemans, A. *J. Am. Chem. Soc.* **2003**, *125*, 9750−9760. (b) Mironov, V. S.; Chibotaru, L. F.; Ceulemans, A. *Phys. Rev* B. **2003**, *67*, 14424−14428.

system a degenerate doublet that is split in the presence of an applied magnetic field by the Zeeman energy $\beta(g_{a,x}+g_{b,x})B_x \approx \beta(17.8)B_x$, which is consistent with the experimental result for **1a**, 16(2) (the very small zero-field splitting Δ has not been included in eq 3 for the sake of simplicity).[18] In ref 3 the ground doublet of Fe^{I} mononuclear **3** was identified as the state $|S = {}^3/_2, M_S = \pm{}^3/_2\rangle$; the associated $M_S = \pm{}^1/_2$ levels are ca. 150 cm^{-1} above the ground state. This description suggests that the ground state of **1a** is the $M_S = \pm 3$ doublet belonging to the $S = 3$ multiplet. Being a product state formed from the two $M_S = \pm{}^3/_2$ doublets of the local Fe^{I} sites, the $M_S = \pm 3$ doublet would yield the same B_{int} as the ground doublet of the mononuclear species, as observed. Thus, both the *g* value and the internal magnetic field in **1a** are consistent with a formulation, according to which it is a species with iron sites similar to those of the mononuclear complex **3** of which the spins are coupled ferromagnetically.

Let us now consider the spin state of complex **1a** from the perspective of Anderson's theory for the indirect ("super") exchange coupling between two high-spin $S = {}^3/_2$ Fe^{I} (d^7) ions mediated by a diamagnetic ligand bridge.[19] In this theory the coupling between two paramagnetic sites with spins S_a and S_b is described by the effective Hamiltonian $J\boldsymbol{S}_a\cdot\boldsymbol{S}_b$ in which the coupling constant *J* is expressed as a sum of a ferromagnetic, "potential exchange" contribution and an antiferromagnetic, "kinetic exchange" contribution: $J = J_F + J_{AF}$. The *xy*, *xz*, and x^2-y^2 orbitals (see Figure 7 for convention of axes) of the iron sites in **1a** accommodate unpaired electrons. These three orbitals are part of the antiferromagnetic exchange pathways $xy_a-\pi_y-xy_b$, $xz_a-\pi_z-xz_b$, and $(x^2-y^2)_a-\sigma-(x^2-y^2)_b$ of the $Fe_a-N_2-Fe_b$ moiety.[20] The ferromagnetic term, J_F, which originates from electronic interactions in cross pathways such as xz_a, ..., xy_b, is usually substantially smaller in magnitude than J_{AF}, particularly in the case of linear bridges.[21] Thus, given the linearity of the bridge, complex **1a** is expected to be a molecular antiferromagnet with an $S = 0$ ground state ($J > 0$). However, our Mössbauer spectra indicate that complex **1a** is a paramagnetic system with a quasi-doublet as ground state, showing that $S > 0$. [An isolated ground doublet may arise from an integer spin multiplet through zero-field splitting DS_x^2 with $D < 0$, e.g., $|S = 3, M_S = \pm 3\rangle$, but that situation would require that the coupling is ferromagnetic ($J < 0$).] The superexchange interaction in **1a** passes through the two atoms of the N_2 molecule and is therefore expected to be weak and to yield low-lying excited states. However, the Mössbauer data exclude the presence of excited states within 110 cm^{-1} of the ground doublet.[22] As it appears to be unlikely that the ferromagnetic ordering of the iron spins in **1a** results from potential exchange (J_F), we have searched for an alternative mechanism for explaining the spin state in this complex. In these efforts we have used DFT calculations for complex **1a** and simplified models suggested by these calculations.

4.3. Density Functional Theory Calculations. 4.3.1. Orbital Structure. Figure 6 presents a schematic representation of the basic features of the electronic structure of complex **1a** as obtained from the DFT analysis of the $S = 3$ state. Indicated are the levels with predominant Fe(3d) or N(π) character. The 3d spin−orbitals appear in the calculation for the ferromagnetically ordered spin state as delocalized, $d_a{}^{\alpha}\pm d_b{}^{\alpha}$ and $d_a{}^{\beta}\pm d_b{}^{\beta}$ combinations but can be localized by a unitary transformation without changing the multielectronic wave function because the two $\pm$ orbitals are either both occupied or empty. The intra-atomic exchange interactions lower the majority spin−orbitals d^{α} relative to the minority spin−orbitals d^{β} in energy by ca. 1.3 eV. The exchange polarization shifts the d^{α} energies into the energy range of the occupied N−N bonding $(\pi_{y,z})^{\alpha}$ orbitals so that they effectively mix with them, while the higher-lying d^{β} orbitals predominantly interact with the empty N−N antibonding $\pi^*_{y,z}$ orbitals. For symmetry reasons, the $\pi_{y,z}$ orbitals interact only with the − combinations and do not change the energy of the + combinations, whereas the $\pi^*_{y,z}$ orbitals interact with the + combinations and do not affect the energies of the − combinations.

Table 1 lists key structural parameters obtained by DFT geometry optimizations. The results are in good agreement with the experimental data. We also performed a number of single-point calculations to monitor the changes in the electronic structure as a function of $Fe-N_2$ distance.

For large $Fe-N_2$ separations, the system $Fe_a\cdots N_2\cdots Fe_b$ has the electron distribution $d_a{}^7-(\pi^*)^0-d_b{}^7$, in which there is virtually no back-donation into the π^* orbitals of the dinitrogen ligand, and the local spins are $S_a = S_b = {}^3/_2$, as expected for low-coordinate Fe^{I} sites. The d^7 configuration for an Fe^{I} site is $|(z^2)^2(yz)^2(xz)^{\alpha}(x^2-y^2)^{\alpha}(xy)^{\alpha}|$ and accommodates two d^{β} electrons in z^2 and *yz* orbitals, which are essentially nonbonding and therefore quasi-degenerate.[23] At this juncture it is worthwhile to compare the spin−orbit coupling of the d^7 configuration with that of the corresponding $S = 2$ d^6 configuration, $|(z^2)^2(yz)^{\alpha}(xz)^{\alpha}(x^2-y^2)^{\alpha}(xy)^{\alpha}|$. The spin−orbit interactions of this state involve primarily the excitation of the $(z^2)^{\beta}$ electron into $(yz)^{\beta}$ because the excitation energy for this transition is small in our diketiminate complexes. As a consequence, spin−orbit coupling mixes these states effectively and yields a ground state in which the orbital angular momentum is essentially unquenched along *x* ($\langle L_x\rangle = \pm\sqrt{3}$ if z^2 and *yz* are degenerate). The situation just described occurs in the $LFe^{II}X$ (X = CH_3, Cl^-) complexes analyzed by Andres et al.[2] For the $S = {}^3/_2$ d^7 $|(z^2)^2(yz)^2(xz)^{\alpha}(x^2-y^2)^{\alpha}(xy)^{\alpha}|$ configuration, the situation is quite different, as the energy gap between the highest occupied d^{β} orbital (*yz* in Figure 7) and the lowest unoccupied d^{β} orbital (x^2-y^2 in Figure 7) is sufficiently large (ca. 5000 cm^{-1} estimated by TD DFT of **1a**) to effectively quench the orbital angular momentum. Our Mössbauer analysis has revealed that the iron sites of **1a** have a large (essentially unquenched) angular momentum, invalidating the d^7 case.

We consider now the case of short $Fe-N_2$ distances, yielding the system $Fe_a-N_2-Fe_b$. When the $Fe-N_2$ distance is reduced

(18) While eq 3 describes properly the ground doublet of **1a**, a true Ising Hamiltonian would predict an excited doublet that is not split by a magnetic field, since $\Delta_{Zeeman} = \beta(g_{1,x} - g_{2,x})B = 0$.

(19) Anderson, P. W. In *Magnetism*; Rado, G. T., Suhl, H., Eds.; Academic Press: New York, 1963; Vol. 1 and references therein.

(20) (a) Kahn, O. *Molecular Magnetism*; VCH Publishers: New York, 1993; Chapters 7−9. (b) Bencini, A.; Gatteschi, D. *EPR of Exchange Coupled Systems*; Springer-Verlag: Berlin, Heidelberg, 1990; Chapter 1.

(21) (a) Kahn, O. *Adv. Inorg. Chem.* **1995**, *43*, 179−259. (b) Kahn, O. *Proceedings of the Indian National Science Academy, Part A: Physical Sciences*; **1986**; Vol. 52, pp 875−85. (c) Kollmar, C.; Kahn, O. *Acc. Chem. Res.* **1993**, *26*, 259−265.

(22) Even the magnetic substates $M_S = \pm 2, \pm 1$ of the $S = 3$ ground manifold are elusive.

(23) The $Fe-N_2$ bond stretch weakens also the σ interaction of the x^2-y^2 orbital with the dinitrogen so that eventually this orbital will merge with the z^2/yz ground state to form a quasi-degenerate triplet.

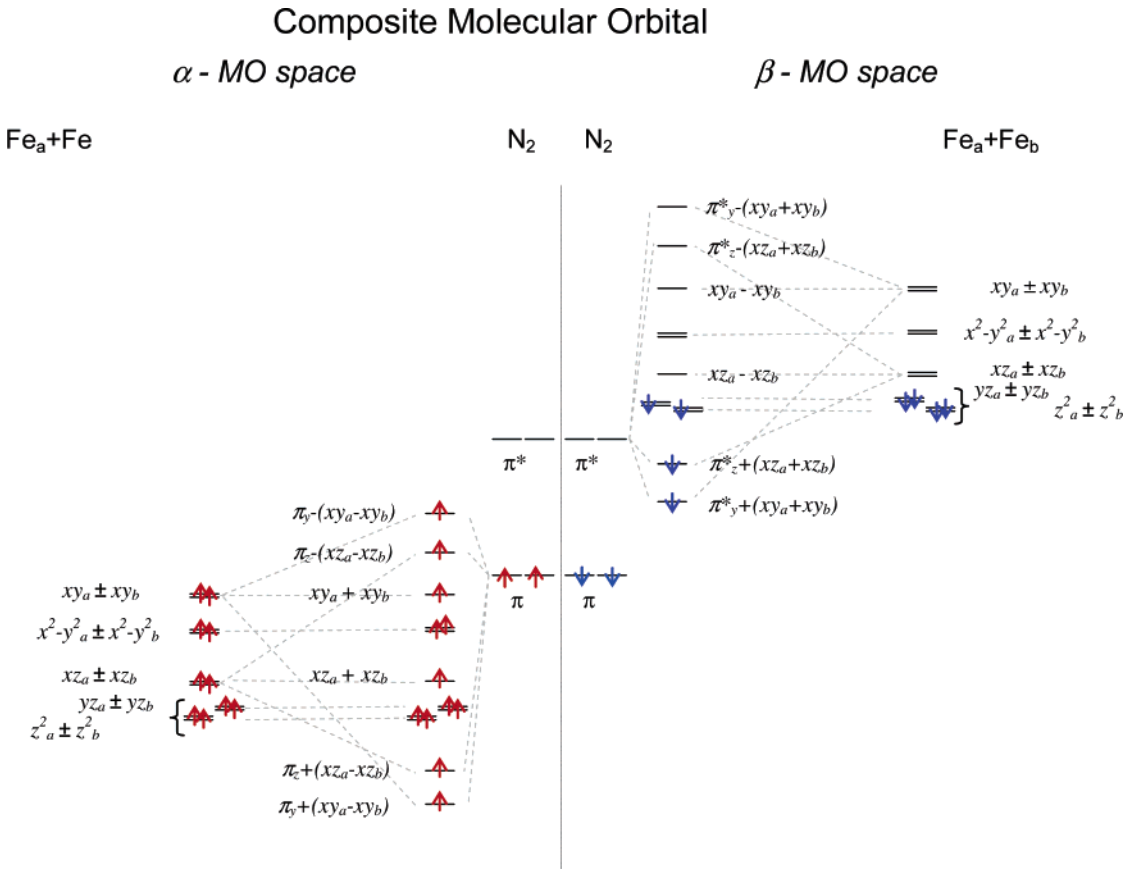

Figure 6. Schematic molecular orbital diagram for complex **1a** (see text).

Table 1. Bond Distances from Experiment and DFT Optimized Structure for an Idealized Model[c] of **1A**

system	Fe–N$_{dik}$[a] [Å]	Fe–N(N$_2$)[b] [Å]	N=N [Å]
exp **1a**	1.746	1.950	1.186
LFeNNFeL $z^2_a \pm z^2_b$	1.758	1.994	1.212
LFeNNFeL $yz_a \pm yz_b$	1.769	1.968	1.214
average	1.763	1.981	1.213

[a] Nitrogen of the diketiminate ligand. [b] Nitrogen of dinitrogen unit. [c] Results for various models are presented in SI.

to the value found for the geometry optimized structure (Fe−N ≈ 1.76 Å), the electronic structure undergoes a profound transformation. Thus, each iron donates one of its d$^\beta$ electrons to N_2, yielding in effect an oxidation state that is better described as (idealized) Fe^{II}−N_2^{2-}−Fe^{II}, with the configuration d_a^6−$(\pi^*)^2$−d_b^6 in which the donated electrons are accommodated in the $\pi^*_{x,y}$ orbitals of N_2. Concomitantly, there is a lengthening of the N_2 bond and a lowering of the π^* levels that shifts them below the minority spin 3d$^\beta$ orbitals with the same symmetry (see Figure 6). As a consequence, the bonding combinations resulting from the interactions of $\pi^*_y{}^\beta$ ($\pi^*_z{}^\beta$) and xy^β (xz^β) have predominant π^* character and favor a configuration in which one of the $(z^2)^\beta(yz)^\beta$ electrons of each iron is effectively transferred to the π^* orbitals of N_2 (the lowest two orbitals in Figure 7); the corresponding antibonding combinations have predominant 3d character and are empty. The π^* nature of the acceptor orbitals can be discerned from the two contour plots at the bottom of Figure 7. Idealized, the local spins for the electronic ground state at the equilibrium conformation are $S_a = S_b = 2$ and $S_c = 1$ (S_c is the electronic spin of N_2^{2-}), the triplet state for N_2^{2-} being analogous to the ground state of the iso-electronic O_2 molecule. The d^6 configuration of each iron is $|[(z^2)(yz)]^3(xz)^\alpha(x^2-y^2)^\alpha(xy)^\alpha|$ and has one d$^\beta$ electron in a quasi-degenerate z^2/yz pair. As in LFe^{II}X, **2**, the small energy gap between z^2 and yz gives rise to a large, unquenched orbital angular moment along molecular axis, x. Associated with the orbital angular moment is an internal magnetic field at the ^{57}Fe nucleus, which couples to the nuclear spin. In the framework of the spin-Hamiltonian formalism, this coupling can be represented as $A_xS_{a,x}I_x$ ($B_{\text{int},a} = -\langle S_{a,x}\rangle A_x/g_n\beta_n$), where A_x is a positive valued magnetic hyperfine coupling constant. This prediction is in accord with the Mössbauer analysis given above. The orbitals z^2 and yz are closely spaced because they are essentially nonbonding. The nonbonding nature of these orbitals is supported by the similarity of the structures obtained from geometry optimizations for configurations in which either the z^2 or yz orbital is doubly occupied (see Table 1).

Complex **1a** presents favorable conditions for electron transfer from Fe to N_2 and thus for the activation of the dinitrogen moiety, namely: (i) the presence of a seventh 3d electron in valence shell of Fe^I raises the orbital energies relative to those for Fe^{II}, destabilizing the d^7 configuration, and (ii) the $S_c = 1$ configuration $(\pi^*_y)^\beta(\pi^*_z)^\beta$ is lowered in energy by the exchange interaction between the two π^* electrons and the lengthening of the N_2 bond. Figure 6 should be considered with the caveat that the orbital energies depend on both the electronic configuration and the structure. In the $S_c = 1$ (Fe^{II}N_2^{2-}Fe^{II}) configuration the π^* energies are raised by the Coulombic repulsion between the two π^* electrons but are substantially lowered by the exchange interaction between them, by the bonding interac-

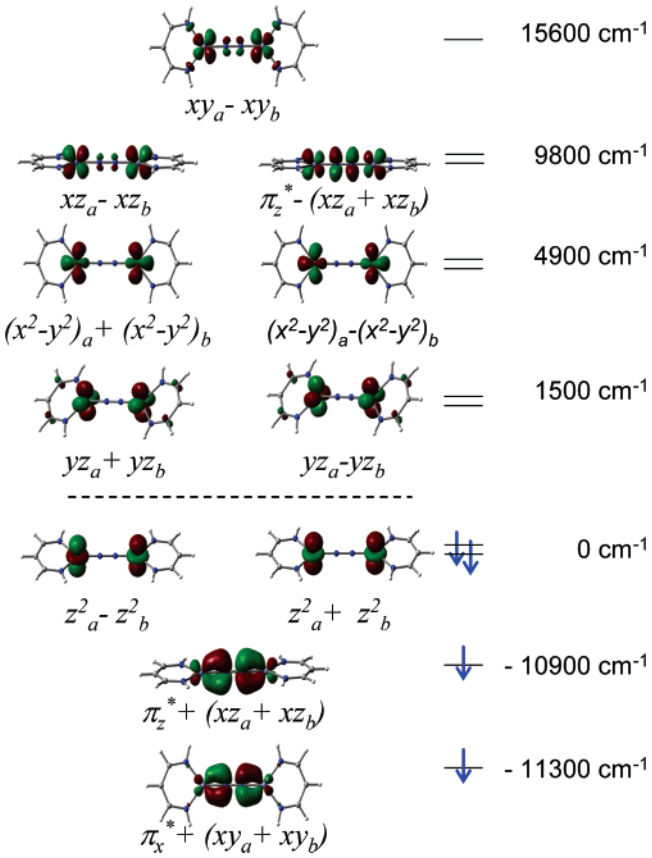

Figure 7. Contour plots of the upper orbitals for the β electrons derived from TD-DFT calculations. The axes are chosen such that x is along the Fe−NN−Fe axis, the y axis is in the same plane and parallel to the nitrogen atoms of the diketiminate ligands, and the z axis is orthogonal to the plane of the diketiminate ligands. These plots are for a simplified model of **1a** with an idealized D_{2h} point group symmetry (more information is given in Supporting Information).

tions of the π^* orbitals with the 3d orbitals of the Fe^{II} sites, and by the lengthening of the N_2 bond. Obviously, a quantitative prediction about the relative energies of electronic configurations can only be made by comparing the total energies at their equilibrium structures.[24]

4.3.2. DFT Results for Electric Field Gradient Tensor and Isomer Shift. Table 2 lists the values for the isomer shift, the quadrupole splitting and the asymmetry parameter, η, of **1a** from Mössbauer analysis and DFT calculations of the idealized $Fe^{II}-N_2^{2-}-Fe^{II}$ complex. Also given are the components, V_{xx}, V_{yy}, and V_{zz}, of the electric field gradient (EFG) tensor, which is diagonal in the coordinate frame (x,y,z). The computed values were evaluated for both the $\{z^2\}$ and $\{yz\}$ orbital configuration of the Fe^{II} ions. Adopting the (standard) notation V_{max}, V_{mid}, and V_{min} with $|V_{max}| \geq |V_{mid}| \geq |V_{min}|$ for the three EFG components, the asymmetry parameter and quadrupole splitting can be expressed as $\eta = (V_{mid} - V_{min})/V_{max}$ and $\Delta E_Q = (eQV_{max}/2)\sqrt{(1 + \eta^2/3)}$. As shorthand we use in the following discussion the notation V' for $eQV/2$. The Mössbauer spectra afford accurate determinations of the EFG component along the easy magnetization axis, x, and of ΔE_Q, and thus of all three components as $V_{xx}+V_{yy}+V_{zz} = 0$. It is important to note that the Mössbauer analysis not only provides the magnitudes of the EFG components but also the signs of these quantities. The

(24) For this purpose we use the total energy of the DFT state.

Table 2. Experimental (bold) and DFT Results for the EFG Tensors and Isomer Shifts of **1a** and Mononuclear Fe^{II} and Fe^{I} Diketiminate Complexes (Averages Due to Spin−Orbit Coupling Are Given in Italics)

	EFG components[a]			MB parameters[b]		
model config/orbital	x	y	z	η	ΔE_Q	δ
LFeNNFeL $z^2_a \pm z^2_b$	−1.71	1.60	0.11	0.87	−1.91	0.39
LFeNNFeL $yz_a \pm yz_b$	0.47	−2.3	1.84	0.59	−2.44	0.58
LFeNNFeL average	*−0.62*	*−0.35*	*0.97*	*0.27*	*0.97*	*0.49*
LFeNNFeL exp (1a)	**−1.00**	**−0.35**	**1.35**	**0.48**	**1.41**	**0.62**
$LFe^{II}CH_3$ z^2	−1.54	1.69	−0.14	0.83	1.87	0.23
$LFe^{II}CH_3$ yz	0.36	−2.20	1.84	0.67	−2.36	0.41
$LFe^{II}CH_3$ average	*−0.59*	*−0.26*	*0.85*	*0.39*	*0.87*	*0.32*
$LFe^{II}CH_3$ exp[c]				**0.2**	**1.74**	**0.48**
$LFe^{II}Cl$ z^2	−0.94	1.61	−0.66	0.17	1.61	0.47
$LFe^{II}Cl$ yz	1.80	−2.98	1.19	0.20	−3.00	0.65
$LFe^{II}Cl$ average	*0.42*	*−0.69*	*0.26*	*0.24*	*−0.69*	*0.56*
$LFe^{II}Cl$ exp				**0.5**	**−1.61**	**0.73**
LFe^{I}(HCCH) z^2	−1.06	−0.04	1.11	0.93	1.26	0.50
LFe^{I}(HCCH) yz	1.19	−3.18	1.98	0.24	2.00	0.38
LFe^{I}(HCCH) average	*0.06*	*−1.61*	*1.54*	*1.00*	*−1.86*	*0.44*
LFe^{I}(HCCPh) exp[d]	**0**	**±2.02**	**∓2.02**	**~0.9**	**2.02**	**0.5**

[a] $eQV_{ii}/2$ in mm/s. [b] ΔE_Q and δ in mm/s. [c] Reference 2. [d] Reference 3.

sign of ΔE_Q, which by convention is equal to the sign of V_{max}, is positive in **1a** ($\Delta E_Q = +1.41$ mm/s). The EFG component along the magnetization axis is negative and smaller in magnitude than V_{max} ($V'_{xx} = -1$ mm/s). Hence, $V'_{xx} = V'_{mid} = -1.00$ mm/s, $V'_{min} = -0.35$ mm/s, and V_{max} must be identified with either V_{yy} or V_{zz}, which implies that V_{max} is perpendicular to the magnetization axis (x). To decide between the possibilities $V_{max} = V_{yy}$ and $V_{max} = V_{zz}$, we use the DFT results for the EFG. Table 2 shows that the values calculated for the EFG and ΔE_Q depend significantly on whether the sixth 3d electron is in z^2 or yz; V_{max} is along x and y, respectively. The sign of V_{max} for the two orbital configurations is negative and thus at variance with experiment. The situation changes when we introduce the effect of spin−orbit coupling on the orbital state. Assuming the degenerate case, the two orbital configurations mix as in $(\{z^2\} \pm i\{yz\})/\sqrt{2}$. The EFG tensor for the admixed state is the average of the EFG tensors for the two orbital configurations (see ref 2) and has been listed in Table 2 in italics. The ΔE_Q for the admixed state is obtained from the averaged EFG using the expression given above and has a positive sign. Thus, consideration of spin−orbit coupling yields a ΔE_Q which is positive and perpendicular to the magnetization axis, in agreement with experiment. In particular, the DFT calculation identifies V_{max} with V_{zz}, i.e. the EFG component normal to the diketiminate plane (see Table 2). The same approach has been applied to the mononuclear diketiminate complexes $LFe^{II}X$ (X = Cl^-, CH_3) (ref 2) and LFe^{I}(HCCR) (ref 3) (Table 2). Although not always accurate in predicting the magnitudes of ΔE_Q and η, the DFT/averaging method successfully reproduces the signs and orientations of the ΔE_Q deduced from the Mössbauer data for these species (refs 2,3): (i) In all three complexes V_{max} is perpendicular to the magnetization axis (x, the axis along Fe−X). (ii) ΔE_Q is positive in $LFeCH_3$ and negative in LFeCl. (iii) The component of the EFG along the magnetization axis of LFe(HCCR) is vanishes, $V_{xx} \approx 0$. Since $\eta \approx 1$, $V_{yy} \approx -V_{zz}$ the sign of ΔE_Q is undefined in this case.

The EFG can be decomposed into contributions for the valence electrons in the d^6 shell of the iron and for the ligand electrons: $V = V_{val} + V_L$. The valence term for the $\{z^2\}$ configuration is (roughly) $(V'_{val,xx}, V'_{val,yy}, V'_{val,zz}) \approx (2, 2, -4)$

mm/s and for $\{yz\}$ we have $V'_{val} \approx (4, -2, -2)$ mm/s. The ligand term for square planar coordination has a positive component along the normal of the molecular plane ($V'_{zz} = V'_{L,max} > 0$) and two negative components in the (x,y) plane ($V'_{L,mid} < 0$ and $V'_{L,min} < 0$) (ref 2). Given that we are considering a complex with an (idealized) N_2^{2-} ligand, there is a significant accumulation of electronic charge along the x axis so that we expect that $V_{L,xx} = V_{L,mid}$ and $V_{L,yy} = V_{L,min}$. For example, if we adopt $V'_L = (-3.5, -0.5, 4.0)$ mm/s then $V'_{val} + V'_L = (-1.5, 1.5, 0)$ mm/s for $\{z^2\}$ and $V'_{val} + V'_L = (0.5, -2.5, 2)$ mm/s for $\{yz\}$. These values are approximately equal to those given in the first two lines of Table 2. Averaging over the EFGs for the two orbital states yields $(V'_{val} + V'_L)_{av} = (-0.5, -0.5, 1.0)$ mm/s, which matches roughly the third line of the table. Notice that the EFG component along the magnetization axis (x) is negative, in agreement with the Mössbauer data. Interestingly, the average over the valence contributions alone, $(V'_{val})_{av} = (3, 0, -3)$ mm/s, yields a large positive component along x. Thus, a large negative ligand contribution is required to obtain the small negative value observed for the EFG along x. Obviously, the N_2^{2-} ligand is the source of this contribution.[25]

The dependence of the isomer shift δ on the details of the d^6 orbital configuration of the Fe^{II} sites is unusual ($\delta = 0.39$ mm/s for $\{z^2\}$ and 0.58 mm/s for $\{yz\}$, see Table 2) but can be explained as follows. For reasons of symmetry the z^2 orbital mixes with the 4s orbital in the crystal field of the molecule, whereas yz does not. An electron in a hybrid z^2-4s orbital gives a higher electron density at the nucleus (and thus a lower value of δ) than an electron occupying a yz orbital. The DFT predictions for the two configurations should be averaged to account for spin−orbit coupling. The resulting value $\delta_{av} = 0.49$ mm/s is somewhat lower than the experimental number (0.62 mm/s), which is not surprising as the models used in the calculations are idealized renditions of the true structure.

4.4. Consideration of Exchange and Spin−Orbit Coupling. 4.4.1. Effective Hamiltonian. The spin part of the DFT ground state can be formulated as $|M_a = 2, M_c = -1, M_b = 2\rangle$ (pictorially: ↑↓↑) and can be viewed as the broken symmetry (BS) approximation for the proper spin state in which the Fe^{II} spins are antiferromagnetically coupled to the N_2^{2-} spin: $|((S_a = 2, S_b = 2)S_{ab} = 4, S_c = 1), S = 3\rangle$, such that the iron spins are aligned parallel. The antiferromagnetic nature of the $Fe-N_2^{2-}$ couplings can be understood with the aid of Figure 6. In the BS configuration the π interactions between N_2^{2-} and the 3d orbitals substantially lower the energies of the $(\pi^*)^\beta$ electrons; the corresponding rise in the $(d_\pi)^\beta$ levels has no effect on the energy because they are empty. The situation changes in the ferromagnetic configuration, $|M_a = 2, M_c = 1, M_b = 2\rangle$ (↑↑↑), in which the transferred electrons occupy the $(\pi^*)^\alpha$ levels, which are located well above the $(d_\pi)^\alpha$ levels (Figure 6) by a considerable margin[26] such that the stabilization energy due to the π interactions for the ferromagnetic configuration ↑↑↑ is less than for the BS configuration ↑↓↑. Moreover, since in this case both the bonding and antibonding orbitals are occupied, the effect of the π interactions on the total energy is diminished by the rise in the energies for the electrons in the antibonding orbitals. The sign of the coupling constants between N_2^{2-} and the Fe^{II} sites, namely $J_{ac} = J_{bc} > 0$, is consistent with the valence-bond theory for exchange interactions, according to which unpaired electrons in non-orthogonal orbitals centered at two interacting paramagnetic sites give rise to antiferromagnetic exchange.[27] Given that we are dealing with neighboring atoms, the "direct" exchange couplings between N_2^{2-} and the irons are expected to be much stronger than the "indirect" exchange coupling between the irons.

The foregoing discussion suggests the effective Hamiltonian eq 4, for describing the energy states of complex **1a**.

$$\mathcal{H} = \mathcal{H}_a^{CF} + \mathcal{H}_b^{CF} + J_{ac}S_a\cdot S_c + J_{bc}S_b\cdot S_c + J_{ab}S_a\cdot S_b + \lambda(L_a\cdot S_a + L_b\cdot S_b) \quad (4)$$

The first two terms represent the crystal-field splittings of the 3d orbitals at the two metal sites, the third and fourth term describe the exchange couplings between the Fe^{II} sites and the N_2^{2-} bridge, the J_{ab} term accounts for the (weak) indirect exchange coupling between the two Fe^{II} sites, and the sixth and seventh term are the spin−orbit coupling operators for the two irons ($\lambda \approx -100$ cm^{-1}). The Hamiltonian acts in the 1875 dimensional product space $(L_a\otimes S_a)\otimes(L_b\otimes S_b)\otimes S_c$ with $L_a = L_b = 2$, $S_a = S_b = 2$, and $S_c = 1$. The crystal-field operators are assumed to be diagonal in the basis of the real 3d orbitals ($d_{k,i} = (z^2)_k, (xz)_k, (yz)_k, (xy)_k, (x^2-y^2)_k$; $k = a$ or b) for the two iron sites,.[28] The symmetry of **1a** implies that $J_{ac} = J_{bc} = J$. We have estimated the value for J from the DFT total energies for the ferromagnetic state (↑↑↑) and the broken symmetry state (↑↓↑), using the expression $J = [E(\uparrow\uparrow\uparrow) - E(\uparrow\downarrow\uparrow)]/8$, and obtained $J = 3500$ cm^{-1}.[29] In principle, the values of the exchange parameters in eq 4 are dependent on the orbital states of the Fe^{II} ion. However, since the β electrons of the Fe^{II} sites occupy the orbitals z^2 or yz, which are nonbonding with respect to the N_2^{2-} bridge, we expect that the influence of the orbital state on the exchange-coupling constants to be weak, and we thus have ignored any such dependence.

The DFT-estimated $J \approx 3500$ cm^{-1} value is considerably larger in magnitude than the spin−orbit coupling constant, $\lambda \approx -100$ cm^{-1}, which prompts us to consider first the exchange part of eq 4. The operator containing the J terms in eq 4 yields eigenstates of the form $|((S_a,S_b)S_{ab},S_c)S\rangle$ with energies

$$E(S_{ab},S) = c + {}^1/_2JS(S+1) + {}^1/_2(J_{ab} - J)S_{ab}(S_{ab}+1) \quad (5)$$

in which the spin quantum numbers fulfill the well-known triangular relationships and c is a constant. Since $|J_{ab}| \ll J$, the ground state is $|S_{ab} = 4, S = 3\rangle$; the lowest excited spin state, $|S_{ab} = 4, S = 4\rangle$, is separated from the ground state by as much as $4J \approx 14\,000$ cm^{-1}. The lowest excitation energies pertain to the 3d transitions $(z^2)^\beta \rightarrow (yz)^\beta$ at the two Fe^{II} sites. The crystal-field splitting between z^2 and yz is in magnitude comparable to the spin−orbit coupling constant, λ, such that this interaction

(25) As in the case of complex **1a**, the nature of the third ligand is also reflected in the V_{xx} values listed for the $LFe^{II}X$ complexes in Table 2. The value of V_{xx} for X = CH_3 is smaller than that for X = Cl^- in both orbital configurations, which indicates that the EFG generated by the strong CH_3 ligand is larger than the one generated by Cl^-.

(26) The effect of the spin polarization on the $(\pi^*)^\alpha$ levels is smaller than on the d^α levels because the former are centered at the dinitrogen ligand.

(27) (a) Curély, J. *Monatsh. Chem.* **2005**, *136*, 1013−1036 (b) Ceulemans, A.; Chibotaru, L. F.; Heylen, G. A.; Pierloot, K.; Vanquickenborne, L. G. *Chem. Rev*, **2000**, *100*, 787−805.

(28) This assumption is supported by TD-DFT calculations.

(29) A straightforward derivation shows that $\langle\uparrow\uparrow\uparrow|JS_{ab}\cdot S_c|\uparrow\uparrow\uparrow\rangle - \langle\uparrow\downarrow\uparrow|JS_{ab}\cdot S_c|\uparrow\downarrow\uparrow\rangle = (n\uparrow)(n\downarrow)J$ with $S_{ab} = S_a + S_b$ and $(n\uparrow)$ is the number of unpaired α electrons in spin ↑ and $(n\downarrow)$ is the number of unpaired β electrons in Fe spin ↓, which yields $4 \times 2 = 8$ in the present case.

mixes the two states effectively. The resulting orbital angular moment is along *x*, because $\langle z^2|l_x|yz\rangle = i\sqrt{3}$ is the only nonvanishing component of the single particle angular momentum operator $\boldsymbol{l}$. As discussed by Andres et al.[2] for the mononuclear $LFe^{II}X$, with ground spin multiplet $|S_a = 2, M_a\rangle$ ($M_a = 0, \pm1, \pm2$), the spin acts, through spin−orbit coupling, as a magnetic field on the orbital moment, $\lambda\langle M_a|S_{a,x}|M_a\rangle L_x \equiv \beta B_x L_x$. The matrix element has the values $M_a = \pm2, \pm1, 0$, provided the spin is quantized along *x* (i.e., $S_x|S_a, M_a\rangle = M_a|S_a, M_a\rangle$). For the degenerate case, $\epsilon(yz) = \epsilon(z^2)$, the spin−orbit interaction yields the orbital states $[(z^2) \pm i(yz)]/\sqrt{2}$ with energies $-|\lambda M_a|\sqrt{3}$, i.e., a sequence of equidistant levels corresponding to $M_a = \pm2, \pm1, 0$, with $M_a = \pm2$ being the ground doublet. As in the mononuclear complex **3**, spin−orbit coupling yields for the three-spin system in complex **1a** an equidistant energy ladder with the states $|S, M_S\rangle$, ($M_S = \pm3, \pm2, \pm1, 0$), $M_S = \pm3$ being the ground doublet, but with a slightly larger splitting between the subsequent levels, $\pm(^5/_4)|\lambda M_a|\sqrt{3}$, due to the coupled nature of system spin *S*. The local orbital moments ($\pm\sqrt{3}\,\beta$) and associated internal magnetic fields ($\pm\sqrt{3}\,\beta\langle r^{-3}\rangle/g_n\beta_n$) of the Fe^{II} in both the mononuclear and dinuclear systems are equal.

4.4.2. Crystal-Field Splitting between z^2 and *yz* versus Orbital Angular Momentum Quenching. Thus far we have considered the case that the *yz* and z^2 levels are degenerate. In fact this condition can be relaxed considerably. The following observations are made when the degeneracy is removed, i.e., for $\epsilon(yz) - \epsilon(z^2) \neq 0$: (a) The ground doublet ($M_S = \pm3$) and the first two excited doublets ($M_S = \pm2, \pm1$) remain strictly degenerate as long as spin−orbit coupling with the excitations $z^2/yz \rightarrow xz$, x^2-y^2, and *xy* is ignored. (b) The orbital angular moment is gradually quenched upon increasing the gap between z^2 and *yz*. This is shown in Figure 8B where we have plotted $\langle L_{a,x}\rangle = \langle L_{b,x}\rangle$ as a function of the ratio $[\epsilon(yz) - \epsilon(z^2)]/|\lambda|$. The unquenched orbital moments of the two irons in the ground doublet give rise to a contribution to the effective *g* value along *x*, g_x; the effective *g*-values along *y* and *z* are zero because the ground doublet $M_S = \pm3$ is strictly axial (Recall that the spin is quantized along *x*). Figure 8C shows a plot of g_x vs $[\epsilon(yz) - \epsilon(z^2)]/|\lambda|$. In the degenerate case, the orbital contributions of the two irons to g_x is $g_{L,x} = 4\sqrt{3}$ and give together, in the language of eq 1, with the spin-only contribution ($g_{s,x} = 4$, $S = 12$) the value $g_x = 12 + 4\sqrt{3} \approx 18.9$ (maximum in Figure 8C). Given the experimental estimate $g_x = 16 \pm 2$ we obtain the condition $3|\lambda| < |\epsilon(yz) - \epsilon(z^2)| < 20|\lambda|$ for the crystal-field splitting between *yz* and z^2; as shown below, the observation of magnetic spectra in zero-applied field implies that $[\epsilon(z^2) - \epsilon(yz)\}/|\lambda| \leq 6$ if $\epsilon(z^2) < \epsilon(yz)$, a suggestion supported by DFT calculations.[30] (c) As shown in Figure 8A the zero-field splittings between the pseudo-doublets decrease with increasing values for $[\epsilon(yz) - \epsilon(z^2)]/|\lambda|$. The M_S dependence of the level energies changes from quasi-linear (for $\epsilon(yz) = \epsilon(z^2)$) to quadratic (for $\epsilon(yz) - \epsilon(z^2) \gg |\lambda|$). In the latter limit the zero-field splittings are described by the standard spin Hamiltonian $D_x S_x^2$ term which is rooted in second-order perturbation theory. Parts A and B of Figure 8 were obtained by diagonalizing the Hamiltonian of eq 4 in the full, 1875-dimensional space of states (for details, see Supporting Information).

At the end of the Results section we commented on the temperature dependence of B_{int} at temperatures below 60 K.

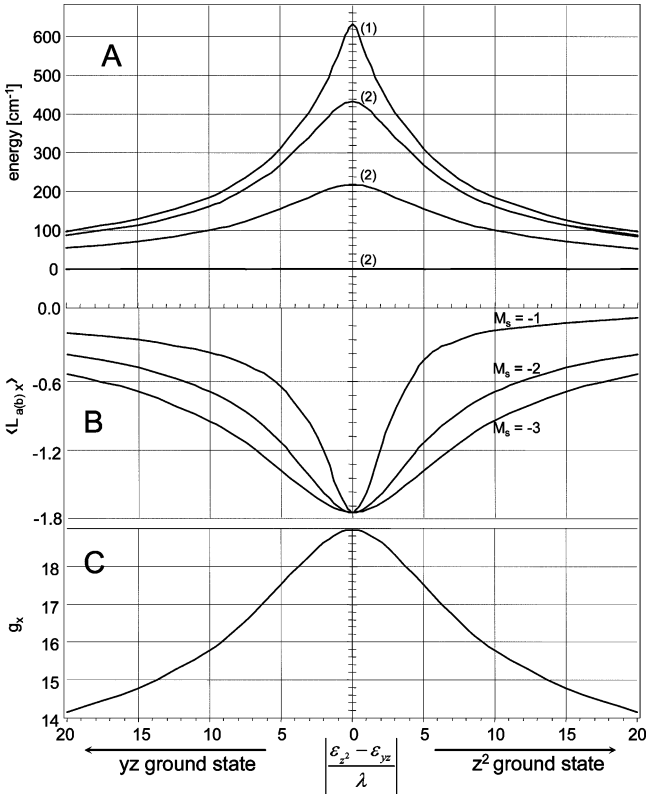

Figure 8. (A) Plot of the energies of the seven lowest states vs $|(\epsilon(z^2) - \epsilon(yz))/\lambda|$. The multiplicities of the levels are indicated in parentheses. (B) Plot of the $\langle L_{a(b),x}\rangle$ expectation values for the $M_S = -3, -2$ and -1 levels with $B = 0.1$ T applied along *x*; for the $M_S = +1, +2, +3$ levels $\langle L_{a(b),x}\rangle$ has the same magnitude but opposite sign. (C) g_x, of the ground doublet calculated in the effective spin $S = {}^1/_2$ representation. Values used: $\epsilon(z^2) = 0$, $\epsilon(xz) = \epsilon(xy) = \epsilon(x^2-y^2) = 2 \times 10^5$ cm^{-1}, $\lambda = -100$ cm^{-1}, and $J_{ab} = J_{bc} = 3500$ cm^{-1}.

For $\epsilon(z^2) = \epsilon(yz)$ our model yields $\langle L_x\rangle = -\sqrt{3}$ for all states with negative M_S and $\langle L_x\rangle = +\sqrt{3}$ for the levels with positive M_S (Figure 8B). Ignoring the small spin-dipolar term, the internal field can be written as $B_{int} \approx P(\langle L_x\rangle - \kappa\langle S_x\rangle)$, where $P = 2\beta\langle r^{-3}\rangle$ and $\kappa \approx 0.15-0.4$ is a scaling factor for the Fermi contact (FC) term. Since $\langle S_x\rangle$ is smaller for the excited states, $\kappa P\langle S_x\rangle$ will decline while $\langle L_x\rangle$ will stay constant when $\epsilon(z^2) = \epsilon(yz)$. Thus, the thermally averaged internal field, $\langle B_{int}\rangle_{therm}$, should *increase* as the temperature is raised, in contrast to what is observed experimentally. However, if we allow some crystal-field splitting between z^2 and *yz*, the $|\langle L_x\rangle|$, values will be smaller for the $M_S = \pm2$ and ±1 levels than for the $M_S = \pm3$ ground levels. To observe a decrease in B_{int} with increasing temperature, $\langle B_L\rangle_{therm}$ must decline faster than $\langle B_{FC}\rangle_{therm}$. This is the case for $|\epsilon(z^2) - \epsilon(yz)| > 5|\lambda|$. It is difficult to obtain a good estimate for the

(30) Although we can presently not prove it, the energy gap between z^2 and *yz* is probably smaller than $6|\lambda|$. The internal field of the Fe^{II} complex **2**−CH_3, $B_{int} = +82$ T observed for the $M_S = -2$ state, reflects the degenerate case $\epsilon(z^2) = \epsilon(yz)$ based on the observation that the experimental $g_x = 11.4$, determined by parallel-mode EPR, agrees with the theoretical estimate $g_x = 11.4$ obtained for the degenerate case.[2] We can relate the experimental value B_{int}(**1a**) = +68.3 T observed for the $M_S = -3$ level of the coupled system to the intrinsic field of the $M_S = -2$ level of an uncoupled local $S = 2$ Fe^{II} site in **1a**, by B_{int}(uncoupled Fe^{II} in **1a**) = $(^2/_3)(^8/_5)$ B_{int}(**1a**) = +72.8 T (the factor $^2/_3$ is the ratio of M_S values and the factor $^8/_5$ is a spin projection factor, ref 18 b, in our 3-spin model). B_{int}(uncoupled Fe^{II} in **1a**) is only 11% smaller than the internal field observed for **2**−CH_3. Reference to Figure 8C, or to Figure 9 of ref 2, suggests that $|(\epsilon(z^2) - \epsilon(yz)| < 6|\lambda|$. The preceding argument ignores possible changes in the Fermi contact and spin-dipolar contribution to B_{int}. The latter contributes ca. 5 T to B_{int} in **2**−CH_3 but is very difficult to estimate for **1a** because it depends crucially on the quantity we wish to estimate, namely the gap between z^2 and *yz*.

energy of the $M_S = \pm 2$ levels because additional unknowns (such as P and κ) enter the calculations. Nevertheless, the observation of a decrease in B_{int} rules out the possibility that z^2 and yz are strictly degenerate; they are probably split by roughly 500 cm^{-1}.

4.4.3. Comment on Spin of 1a. We have argued above that **1a** has an $S = 3$ ground state. In Results we showed that the internal magnetic fields, and therefore the spins, of both iron sites are parallel. When both iron sites are treated as $S = {}^3/_2$ Fe^I, parallel spin alignment will yield an $S = 3$ ground state. As discussed above, strong ferromagnetic coupling between two Fe^I sites is rather unlikely, and therefore, given the large spin density at the dinitrogen bridge indicated by DFT, we developed the 3-spin model. In this model the Fe spins are aligned parallel through direct exchange of two $S = 2$ Fe^{II} with the $S = 1$ N_2^{2-} bridge. This interaction is very strong ($J \approx 3500$ cm^{-1}) and strongly promotes an $S = 3$ ground state. Both models are consistent with $g_x \approx 16$ (see Results and Figure 8C)

The reader may wonder why we have not attempted to verify the spin of **1a** by means of magnetic susceptibility measurements. Aside from the fact that all our samples of **1a** contained a substantial amount of unknown paramagnetic impurities (easily handled in the analysis of the Mössbauer spectra), the value of S cannot be extracted from a powder susceptibility measurement without prior knowledge of (i) the large orbital contribution to the magnetic moment and (ii) the very large zero-field splitting. The conventional spin-only analysis of the susceptibility data would yield a spurious value for the spin.

4.4.4. Zero-Field Splitting of the Ground Doublet. Finally, we consider the spin−orbit coupling involving 3d orbitals other than z^2 and yz, interactions that have been ignored so far. Our TD-DFT calculations show that the (xz), (xy), and (x^2-y^2) levels are separated from the quasi-degenerate $\{z^2,yz\}$ pair by crystal-field splittings larger than 4000 cm^{-1}, and they have therefore a minor influence on the magnetic properties of the ground doublet. The splitting of the ground doublet, Δ, vanishes for $\epsilon(z^2) < \epsilon(yz)$. For $\epsilon(z^2) > \epsilon(yz)$, eq 4 yields $\Delta = 0.0006$, 0.004, and 0.012 cm^{-1} for $[\epsilon(z^2) - \epsilon(yz)\}/|\lambda| = 5$, 10, and 15, respectively. With the preceding information we can specify the conditions for observing, in zero-applied field, paramagnetic hyperfine structure in the low-temperature spectra of **1a**. Figure 2 of Surerus et al.[31] (also pertaining to an $S = 3$ system) shows that fully developed paramagnetic hyperfine structure will be observed for **1a** if $\Delta < g_n\beta_n B_{int}/3 = 0.001$ cm^{-1}. Thus, provided z^2 is the lowest state or $[\epsilon(z^2) - \epsilon(yz)]/|\lambda| \leq 6$, paramagnetic hyperfine structure will be observed for **1a** at 4.2 K even in the absence of an applied field.[30] Finally, we note that the magnetic hyperfine structure observed for solid **1a** in zero field is not a solid-state effect. As shown in Figure S4 the same phenomenon is observed when **1a** is dissolved in methylcyclohexane.[32]

4.5. Relation with Earlier Work. In an earlier DFT study it was demonstrated that the weakening of the N−N bond in the orthogonal conformation of the complex (**1c** in Figure 1) is due to π back-donation.[7] In the present work we have shown that the transfer of electrons into the π^* orbitals of N_2 is essential for the parallel alignment of the iron spins. However, our results differ from those of the MCSCF calculations conducted by Cundari et al.[5,7] in that our DFT solution has a negative, rather than a positive, spin density at the N_2 bridge. Moreover, the low-lying excited states reported in the MCSCF study have spin quantum numbers different from the ground-state spin ($S = 3$), and therefore, the spin−orbit interaction between these states and the ground state is ineffective as a mechanism for unquenching angular orbital momentum. The back-donation into one of the π^* orbitals of acetylene in the mononuclear Fe^I complex, **3**, involves, unlike in the case of **1a**, nearly equal transfers of α and β spin density and generates only an insignificant spin density at the ligand.[3] Delineating the origins of these differences is a subject for future investigations.

Acknowledgment. This work was supported by NSF Grant MCB-0424494 (E.M.) and NIH Grant R01 GM65313 (P.L.H.).

Note Added in Proof. An unrestricted Hartree-Fock calculation (UHF/6-311G) for $M_S = 3$ at the B3LYP/6-311G optimized geometry of model 1 yields a spin population of −1.85 for the N_2 bridge and populations of 3.9 for the two irons. These results corroborate the three-spin model proposed in the text.

Supporting Information Available: Section S1: details of the DFT calculations on selected models and geometric conformations; Section S2: two zero-field Mössbauer spectra of **1a**. This material is available free of charge at http://pubs.acs.org.

JA062051N

(31) Surerus, K. K.; Hendrich, M. P.; Christie, P.; Rottgardt, D.; Orme-Johnson, W. H.; Münck, E. *J. Am. Chem. Soc.* **1992**, *114*, 8579−8590.

(32) Our Mössbauer studies of complex **1c** (not presented) have shown that the electronic ground state of **1c** is very similar to that of **1a**. Thus, paramagnetic hyperfine structure, and a large and positive B_{int}, is observed even in zero field (see Figures S4 and S5). However, in contrast to the well-defined spectra obtained here, B_{int} of complex **1c** was distributed (we have studied 20 samples) over a broad range of values, $(B_{max}-B_{min})/B_{max} \approx 0.3$ indicating a conformational distribution that leads to a dispersion of the orbital energy gap between z^2 and yz. The heterogeneities observed for **1c** prompted us to modify the peripheral groups of the diketiminate ligand, a search that yielded **1a**.